Eur. Phys. J. A **21**, 265–271 (2004)
DOI 10.1140/epja/i2003-10211-3

THE EUROPEAN PHYSICAL JOURNAL A

Neutron excess in analytical expressions for fusion barrier parameters

N.G. Nicolis[a]

Department of Physics, The University of Ioannina, Ioannina 45110, Greece

Received: 1 April 2003 / Revised version: 31 January 2004 /
Published online: 10 August 2004 –
Communicated by A. Molinari

Abstract. The neutron excess dependence of heavy-ion fusion barriers is investigated, guided by predictions of different ion-ion potentials. We develop phenomenological expressions for the fusion barrier radii and heights, involving both the entrance channel mass asymmetry and neutron excess of the projectile and target. Compared to commonly used formulas, the developed expressions reproduce theoretical barrier parameters with a higher accuracy. Furthermore, they provide a means to assess the importance of the neutron excess degree of freedom implied by each potential.

PACS. 24.10.-i Nuclear reaction models and methods – 25.70.-z Low and intermediate energy heavy-ion reactions – 25.70.Jj Fusion and fusion-fission reactions – 25.60.Pj Fusion reactions

1 Introduction

The advent of radioactive beam facilities has opened new frontiers in studies of nuclear structure and reactions [1]. Fusion reactions involving nuclei with an extreme neutron excess result in the synthesis of new nuclear species farther away from the valley of nuclear stability [2]. This effort is expected to enhance the knowledge gathered from the large amount of data already accumulated from studies with stable beams [3,4].

Fusion excitation functions are often analyzed with the classical sharp-cutoff expression $\sigma_{\rm fus}(E) = \pi R_b^2(1-V_b/E)$, where E is the bombarding energy in the center-of-mass system. This expression assumes strong absorption between the interacting nuclei and involves the barrier radius R_b and height V_b. The barrier radius is defined as the distance at which the nuclear attraction balances the Coulomb repulsion, and the barrier height as the sum of nuclear plus Coulomb potential in a head-on collision. Systematic studies of experimental fusion excitation functions have resulted in parametrizations of fusion barrier parameters R_b and V_b [3,4]. These parametrizations provide valuable guides for the assessment of fusion cross section measurements and aid the design of new experiments.

From the theory point of view, the aforementioned expression can be used for the prediction of fusion excitation functions. For example, in refs. [5,6] fusion barrier parameters have been calculated within the sudden approximation, using the Skyrme interaction energy density formalism for closed- and unclosed-shell nuclei. Simple analytical expressions have been obtained for the barrier radii and heights. The calculated excitation functions were in good agreement with experimental data. Furthermore, this procedure was found consistent with the alternative approach of parametrizing the energy density nuclear potential and deducing next the barrier parameters and excitation functions [6].

We note that parametric expressions employed in the literature for R_b, include either linear expressions of the form [4,7]

$$R_b = a\left(A_1^{1/3} + A_2^{1/3}\right) + b \tag{1}$$

or [3]

$$R_b = \left(a + b\log_{10}\left(Z_1 Z_2\right)\right)\left(A_1^{1/3} + A_2^{1/3}\right), \tag{2}$$

where a and b are constants, or polynomial expressions of the form [5,6]

$$R_b = \sum_{i=0}^{3} c_i \left(A_1 A_2\right)^i, \tag{3}$$

where c_i are constants. These expressions involve the mass and atomic numbers of the reacting nuclei and make no reference to the neutron excess. Similarly, Coulomb barrier heights are usually parametrized [4,7] by the product of the two charges over an effective radius of the form of eq. (1) or eq. (2). However, a recent systematic study with the Skyrme energy density formalism has shown a linear increase in the barrier radius and a decrease in barrier

[a] e-mail: nnicolis@cc.uoi.gr

height with increasing N/Z ratio of the compound system, in reactions involving Ca and Ni isotopes with a large neutron excess [8]. One may wonder whether some neutron excess term should be included in the above expressions. The need for detailed parametrizations of fusion barrier parameters has been pointed out in the literature [5,6,8,9].

The object of the present paper is to elucidate the role of the neutron excess in these empirical descriptions. For this purpose, we examine the s-wave barrier parameters predicted by different analytic nuclear potentials. The isospin dependence is studied by varying the neutron excess of isobaric pairs of colliding nuclei, starting with symmetric cases involving $N = Z$ nuclei. As a result, we develop parametric expressions for R_b and V_b incorporating the entrance channel mass asymmetry and the neutron excess. A significant improvement is obtained over commonly used expressions for R_b and V_b. Furthermore, by means of the extracted coefficients, these potentials are assessed in terms of their effectiveness in the neutron excess degree of freedom.

2 Construction of an expression for R_b and V_b

We start with a simple exponential (S.E.) nuclear potential of the form

$$V_n(r) = -V_0 \exp\left(-\frac{r - R_0}{a}\right) \tag{4}$$

with parameters [10] $V_0 = 67.0\,\mathrm{MeV}$, $R_0 = r_0(A_1^{1/3} + A_2^{1/3})$, where $r_0 = 1.17\,\mathrm{fm}$, and $a = 0.574\,\mathrm{fm}$. For zero angular momentum, the fusion barrier radius R_b is obtained as the solution of

$$\frac{\mathrm{d}}{\mathrm{d}r}\left(V_n(r) + V_{\mathrm{Coul}}(r)\right)_{r=R_b} = 0, \tag{5}$$

where $V_{\mathrm{Coul}}(r) = Z_1 Z_2 e^2/r$ is the Coulomb potential. The barrier height V_b is given by the total potential at $r = R_b$. Equation (5) leads to a transcendental equation for r, whose solution can be found numerically. Below, we obtain a parametric expression for this solution using fitting arguments.

We consider the barrier radii of a given $N = Z$ projectile incident on $N = Z$ targets. These are well represented by an expression of the form

$$R_b = a' A_t^{1/3} + b' A_t^{-1/3} + c',$$

where the $A_t^{-1/3}$-term facilitates the description of the low-A_t behavior of R_b. Then, we consider different $N = Z$ projectiles incident on the previous targets. Fitting R_b with the previous expression, we realize that the coefficients a', b' and c' have a cubic-root dependence on the projectile mass. This suggests the following expression

$$R_b = a\left(A_p^{1/3} + A_t^{1/3}\right) + b\left(A_p^{-1/3} + A_t^{-1/3}\right) + c.$$

We find that the new coefficients a, b and c have a weak dependence on A_p and A_t, which can be can be minimized

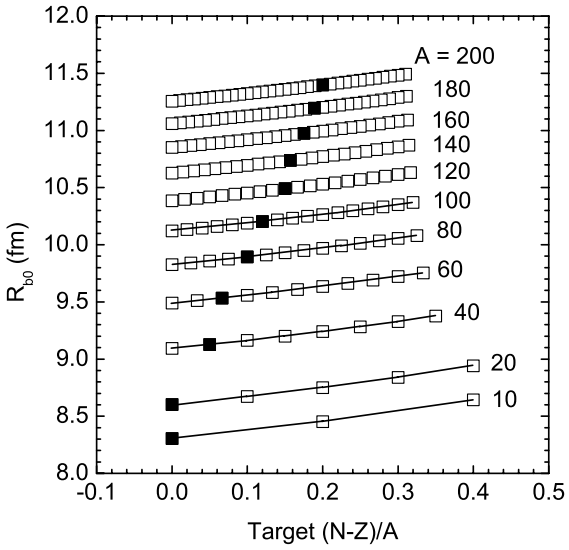

Fig. 1. Barrier radii of ^{16}O projectiles incident on targets with the indicated mass numbers as a function of the relative neutron excess of the targets (open squares). The solid curves guide the eye. Closed squares refer to the barrier radius of targets near the valley of stability.

with the inclusion of two additional terms: one proportional to the reduced mass of the system and another one proportional to the compound nucleus mass. This leads to the expression

$$R_b = a\left(A_p^{1/3} + A_t^{1/3}\right) + b\left(A_p^{-1/3} + A_t^{-1/3}\right) + c\frac{A_p A_t}{A_p + A_t} + d\,(A_p + A_t) + e. \tag{6}$$

Next, we investigate the neutron excess dependence of R_b. For a given $N = Z$ projectile, we vary the neutron and atomic number of the target, keeping a constant $A_t = N_t + Z_t$. A typical example is given in fig. 1, where the exact barrier radii for ^{16}O projectiles (open squares) are plotted *versus* the relative neutron excess of the targets. Target masses ranging from $A = 10$ up to $A = 200$ are shown. The closed squares indicate barrier radii corresponding to targets near the valley of nuclear stability. Here, the relative neutron excess of the targets varies from 0 up to 0.3, which refers to nuclei with $N = Z$ up to the extreme value of $N \approx 1.9Z$, respectively. This range spans a wide region of target nuclei far remote from the valley of nuclear stability. To a good approximation, the dependence of R_b on $\left(\frac{N-Z}{A}\right)_t$ is described with a linear function. A similar behavior was realized for other $N = Z$ projectiles as well. Therefore, for this class of projectile and target combinations we write

$$R_b = f' + g'\left(\frac{N - Z}{A}\right)_t. \tag{7}$$

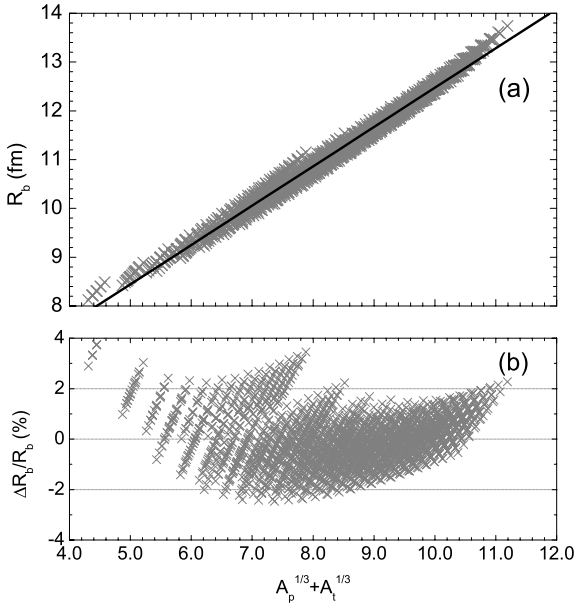

Fig. 2. (a) Barrier radii as a function of $A_p^{1/3}+A_t^{1/3}$. Exact values (crosses) are shown for a large number of projectile-target combinations with a wide range of neutron to proton ratios. The solid line represents a linear fit with eq. (1). (b) Percent differences of the exact values from the linear fit.

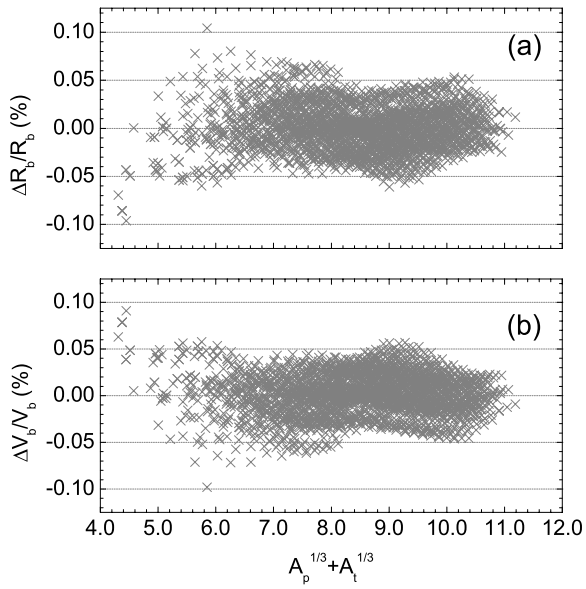

Fig. 3. (a) Percent differences between exact fusion barrier radii and fitted values *versus* $A_p^{1/3}+A_t^{1/3}$. The fit is based on the expression of the present work. A similar plot for V_b is shown in panel (b), where the predicted values are deduced from eq. (11).

The coefficients f' and g' were further examined for a possible projectile mass dependence. Varying the projectile mass number, but still keeping $N_p = Z_p$, we find that the parameter f' is a constant. However, g' was found to vary with A_p as

$$g' = g_1 + \frac{g_2}{A_p},$$

where g_1 and g_2 are constants. Therefore, eq. (7) can be written as

$$R_b = f' + \left(g_1 + \frac{g_2}{A_p}\right)\left(\frac{N-Z}{A}\right)_t . \qquad (8)$$

The coefficient f' was found very close to the barrier radius of the corresponding isobaric pair of nuclei with $N = Z$, given by eq. (6).

As expected from symmetry considerations, a term similar to eq. (8) has to be added with interchanged projectile and target indices. Therefore, we arrive at the following phenomenological expression for the barrier radius of two nuclei with a neutron excess:

$$\begin{aligned} R_b = {} & a(A_p^{1/3}+A_t^{1/3}) + b(A_p^{-1/3}+A_t^{-1/3}) + c\frac{A_pA_t}{A_p+A_t} \\ & + d(A_p+A_t) + \left(e+\frac{f}{A_p}\right)\left(\frac{N-Z}{A}\right)_t \\ & + \left(e+\frac{f}{A_t}\right)\left(\frac{N-Z}{A}\right)_p + g\,. \end{aligned} \qquad (9)$$

For the purpose of testing various expressions, a reference data set was created consisting of numerically calculated barrier radii of all projectile and target combinations with $Z_p, Z_t = 5, 10, 15, \ldots, 70$. The relative neutron excess $\left((N-Z)/A\right)_{p,t}$ was assumed to vary between 0 and 0.2 in steps of 0.05. This corresponds to $N/Z = 1$ up to $N/Z = 1.5$, a range which spans the accessible physical mass regions. Combinations for which the barrier position could not be located, due to the flatness of the potential energy curve, were not considered.

Figure 2(a) shows the exact barrier radii (crosses) of the reference data set plotted as a function of $A_p^{1/3}+A_t^{1/3}$. A linear fit with eq. (1) (solid line) reproduces only the average trend and cannot account for the spread of values, which is a consequence of the large neutron excess range considered. Deviations of the data points about the linear fit are of the order of $\pm 2.0\%$, as shown in fig. 2(b).

Using a multivariate linear regression fit, we determined the coefficients of eq. (9) considered as an equation of a plane surface in 7 dimensions. The percent differences between exact and fitted values of R_b *versus* $A_p^{1/3}+A_t^{1/3}$ are shown in fig. 3(a). The numerical solution of eq. (5) is reproduced to better that $\pm 0.05\%$. This presents a significant improvement over the description made with the simple linear fit.

The quality of a fit can be assessed with a calculated χ^2 per point:

$$\chi^2 = \frac{1}{N}\sum_{i=1}^{N}\left(\frac{R_i^{\rm ex}-R_i^{\rm fit}}{R_i^{\rm ex}}\right)^2 ,$$

where N is the number of data points (projectile-target combinations), and $R^{\rm ex}$, $R^{\rm fit}$ are the exact and fitted value of the radius, respectively. Consecutive fits were performed

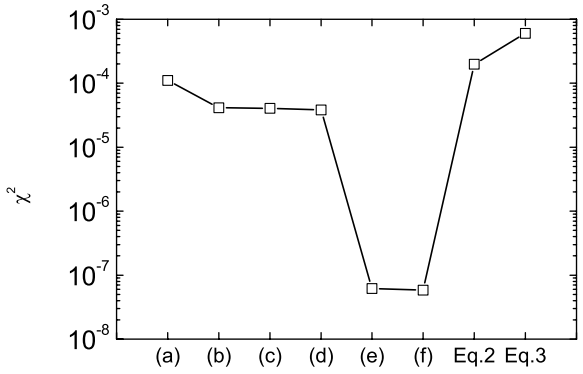

Fig. 4. χ^2 obtained by fitting the reference set of barrier radii with a successively increasing number of terms (a through f) in eq. (9), as well as eqs. (2) and (3).

with eq. (9), starting with the first term and adding one more coefficient at a time, until we arrive to the complete expression. The corresponding values of χ^2 are shown in fig. 4 (a through f). We realize that by adding the terms with coefficients a through d, we obtain a weak decrease in χ^2. Note that case a corresponds to a linear fit with eq. (1). With the inclusion of the neutron excess terms (with coefficients e and f), we obtain a dramatic decrease in χ^2 by 3 orders of magnitude. On the same plot, we show the χ^2 obtained with eqs. (2) and (3) on the same data set. The quality of these fits is similar to or slightly worse than the linear fit with eq. (1). We conclude that the neutron excess terms in eq. (9) produce a substantial improvement in the description of variations in R_b related to the neutron excess of the projectile and/or target.

For a given projectile with $N = Z$ incident on isobaric targets, fusion barrier heights calculated with the above potential show a linear decrease with increasing neutron excess of the target nucleus. This is illustrated in fig. 5, for ^{16}O projectiles incident on isobaric chains of nuclei with the indicated mass numbers. Parametrizations can be obtained in terms of the *equivalent Coulomb radius* $R_{\rm fus}^{\rm Coul}$, representing the distance at which the Coulomb potential equals the barrier height

$$V_b = \frac{Z_1 Z_2 e^2}{R_{\rm fus}^{\rm Coul}}. \tag{10}$$

Alternatively, for an exponential nuclear potential with diffuseness parameter a, one may obtain V_b using the expression [11]

$$V_b = \frac{Z_1 Z_2 e^2}{R_b}\left(1 - \frac{a}{R_b}\right). \tag{11}$$

Using eq. (9) in a multivariate linear regression fit for $R_{\rm fus}^{\rm Coul}$ we obtain an agreement with the numerically calculated barrier heights to better than $\pm 0.05\%$. The same degree of agreement was obtained with the parametrization of R_b, combined with the diffuseness parameter $a = 0.574\,$fm, in eq. (11). The percent deviations from the exact values are shown in fig. 3(b).

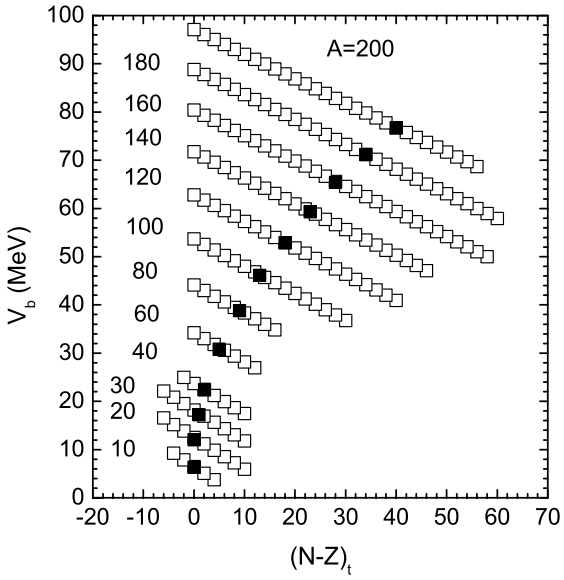

Fig. 5. Barrier heights of ^{16}O projectiles incident on isobaric chains of nuclei with the indicated mass numbers as a function of the neutron excess of the target (open squares). Closed squares refer to the barrier height of targets near the valley of stability.

3 Barrier parameters implied by different nuclear potentials

The coefficients of eq. (9) for R_b and $R_{\rm fus}^{\rm Coul}$ were deduced for the following heavy-ion potentials, listed according to increasing complexity in their functional form.

3.1 The Christensen and Wither potential

The Christensen and Winther potential (C.W.) has been derived in an analysis of elastic-scattering data [7]. It is given by

$$V_n(r) = -S_0 \overline{R}_{12} \exp\left(-\frac{r-R}{a}\right),$$

where

$$S_0 = 50\,{\rm MeV}\cdot{\rm fm}^{-1},$$
$$a = 0.63\,{\rm fm},$$
$$R = R_1 + R_2,$$

with $R_i = \left(1.233A_i^{1/3} - 0.978A_i^{-1/3}\right)$ fm, $(i = 1, 2)$ and $\overline{R}_{12} = R_1 R_2/(R_1 + R_2)$.

The strength of this nuclear potential depends on the projectile and target masses via the reduced radius $\overline{R}_{12}$.

3.2 The proximity potential

The proximity potential [12] (PROX.) predicts the internuclear potential as being due to the separation between

two semi-infinite slabs of nuclear matter, modified by a geometric curvature correction, times an energy density functional $\Phi(\xi)$ of the separation distance ξ (whose analytic expression is given in ref. [13]):

$$V_n = -4\pi\gamma b\overline{R}\Phi(\xi).$$

The reduced radius $\overline{R}$ is defined in terms of the half-density radii of the two nuclei:

$$\overline{R} = \frac{C_1 C_2}{C_1 + C_2},$$

where $C_i = R_i\left[1 - (b/R_i)^2\right]$, with $R_i = (1.28A_i^{1/3} - 0.76 + 0.8A_i^{-1/3})$ fm.

For the diffuseness parameter b, the value $b = 0.99$ fm was used. The separation distance ξ is defined as $\xi = r - (R_1 + R_2)$. For the surface tension γ, we used the liquid-drop surface energy coefficient given by

$$\gamma = 0.9517\left[1 - 1.7826\left(\frac{N-Z}{A}\right)^2\right]\ \mathrm{MeV}\cdot\mathrm{fm}^{-2},$$

where N, Z and A refer to the combined system of the two interacting nuclei.

Here, the nuclear-potential strength has a dependence on the relative neutron excess of the projectile and target, and a mass dependence through the reduced-radius factor.

3.3 The Yukawa-plus-exponential potential

The Yukawa-plus-exponential potential [14,15] (Y.P.E.) satisfies the liquid-drop saturation condition at saturation density. It has the form

$$V_n = -V_{\mathrm{red}}\,(2 + s/a)\exp\left(-s/a\right),$$

where $s = r - (R_1 + R_2)$ is the separation between the equivalent sharp surfaces of the two nuclei (whereas the central radii are used to define s in the proximity model).

In an approximate form, V_{red} is expressed as

$$V_{\mathrm{red}} = \left[c_s(1)c_s(2)\right]^{1/2}\frac{aR_1R_2}{r_0^2\,(R_1 + R_2)}.$$

This is valid when R_1/a, $R_2/a \gg 1$. There are four parameters in this model, namely, the radius parameter r_0, the range of the folding function a, the surface energy constant a_s, and the surface asymmetry constant k_s. The neutron excess dependence of V_{red} is included in the geometric mean of the effective surface energy constants $c_s(i) = a_s\left\{1 - k_s\left[(N-Z)/A\right]^2\right\}$.

In our calculations we used the complete expression for V_{red} together with the model parameters as reported by Möller and Nix [15,16].

3.4 Nuclear potential from the energy density formalism

In ref. [17], the interaction between two heavy ions has been calculated using the energy density formalism (E.D.F.) and Fermi distributions for the nuclear densities. The nuclear part of the interaction potential was found to satisfy the proximity scaling, to a good extent. The functional form of this potential is similar to the proximity potential, apart from the surface coefficient factor. The neutron excess dependence of the projectile and target is introduced through the reduced radius of the system [17].

3.5 Remarks on the deduced coefficients

For the previous nuclear potentials, the fit procedure extended over a common mass region, prepared as described in sect. 3. The deduced coefficients of eq. (9) for the fusion barrier radius and the equivalent Coulomb radius are compiled in tables 1 and 2, respectively. The χ^2 and percent deviations from the exact values of R_b and V_b are also given.

Percent deviations vary between $\pm 0.05\%$ up to $\pm 0.50\%$ for R_b, and between $\pm 0.05\%$ up to $\pm 0.22\%$ for V_b. Therefore, our functional form accounts well for the neutron excess dependence of R_b and $R_{\mathrm{fus}}^{\mathrm{Coul}}$ implied by each heavy-ion potential, despite their differences in the strength of the nuclear attraction. This is not surprising, since the s-wave barrier radius appears in the tail region of the nuclear potential. Differences in the strength of the nuclear attraction show up in the values of the deduced coefficients.

The coefficients a, b, c and d specify the (trivial) mass dependence of R_b and $R_{\mathrm{fus}}^{\mathrm{Coul}}$. On the other hand, the coefficients e and f specify the effectiveness of each potential in the neutron excess of the projectile and/or target. In particular, let us consider a projectile with $N = Z$ incident on a series of isobaric targets. Compared to R_b of the target with $N = Z$, the barrier radius should vary as

$$\Delta R_b = \left(e + \frac{f}{A_p}\right)\left(\frac{N-Z}{A}\right)_t. \qquad (12)$$

The quantity $e + f/A_p$ is a measure of the barrier radius variation with the relative neutron excess of the target. This quantity is plotted in fig. 6 for the nuclear potentials under consideration. Shaded histograms correspond to ^{16}O and the open ones to ^{40}Ca. The first two potentials show a similar behavior. Their neutron excess dependence is equally strong for the light and heavy projectile. However, the C.W. has a stronger dependence than the S.E. potential. In contrast, the other three potentials have a stronger dependence for the heavy than for the light projectile. Among them, the Y.P.E. potential has the strongest dependence. Furthermore, the E.D.F. appears similar to the proximity potential. This is consistent with the similarity of the two potentials in the tail region, despite the differences they exhibit in the inner region, as pointed out in ref. [17].

Table 1. Coefficients and χ^2 for the barrier radius expression.

	Nuclear Potential				
Coefficient	S.E.	C.W.	PROX.	Y.P.E.	E.D.F.
a	0.944	0.961	1.007	1.006	0.877
b	2.553	0.147	1.57	1.9	-0.066
c	-9.755×10^{-4}	3.391×10^{-4}	7.693×10^{-4}	-0.011	-1.98×10^{-3}
d	1.14×10^{-3}	1.422×10^{-3}	1.162×10^{-3}	-1.205×10^{-3}	1.692×10^{-3}
e	0.706	0.783	0.847	1.296	0.822
f	0.269	0.263	-1.836	-4.238	-1.621
g	1.671	2.822	1.269	1.651	4.575
$\chi^2(R_b)$	5.846×10^{-8}	1.551×10^{-7}	1.153×10^{-6}	4.921×10^{-6}	4.012×10^{-7}
$\Delta R_b/R_b$ (%)	± 0.05	± 0.10	± 0.30	± 0.50	± 0.20

Table 2. Coefficients and χ^2 for the effective Coulomb radius expression.

	Nuclear Potential				
Coefficient	S.E.	C.W.	PROX.	Y.P.E.	E.D.F.
a	0.939	0.954	0.973	0.917	0.892
b	2.542	0.15	1.468	1.586	-0.161
c	-9.161×10^{-4}	4.485×10^{-4}	1.268×10^{-3}	-4.059×10^{-3}	-1.277×10^{-3}
d	1.16×10^{-3}	1.452×10^{-3}	1.501×10^{-3}	5.161×10^{-4}	1.684×10^{-3}
e	0.704	0.781	0.834	0.971	0.717
f	0.255	0.229	-1.735	-1.407	-1.121
g	2.319	3.534	2.331	3.125	5.039
$\chi^2(V_b)$	5.029×10^{-6}	1.442×10^{-5}	6.584×10^{-5}	3.628×10^{-5}	2.164×10^{-5}
$\Delta V_b/V_b$ (%)	± 0.05	± 0.09	± 0.22	± 0.18	± 0.15

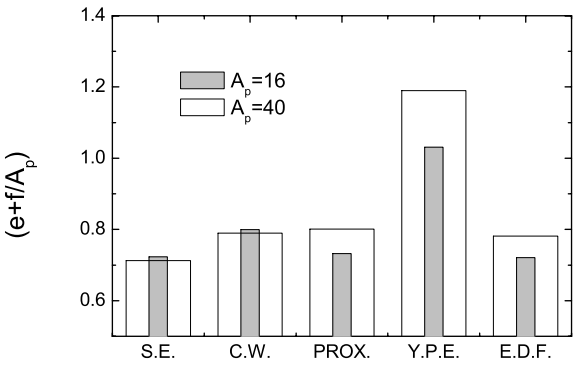

Fig. 6. The neutron excess parameter $(e + f/A_p)$ is shown for the different nuclear potentials examined in the present work. Shaded histograms correspond to ^{16}O and the open ones to ^{40}Ca projectiles.

Similar conclusions can be drawn from an inspection of the quantity $e + f/A_p$ for $R_{\rm fus}^{\rm Coul}$, apart from some weakening of this quantity for the E.D.F. compared to the proximity potential.

4 Discussion

Our results are consistent with an increase in R_b and a decrease in V_b with increasing neutron excess of the reaction partners. This is in qualitative agreement with the results of Puri *et al.* [8], despite the difference of our expression from the functional dependence of R_b, reported in ref. [8]. In this respect, we have to note the work of Christley *et al.*, who have created nuclear densities using a Hartree-Fock approach with Skyrme forces [9]. These calculations show the development of a neutron skin as one moves towards the drip line. The ion-ion potential was obtained by double folding an effective nucleon-nucleon interaction. It was realized that in neutron-rich nuclei, the neutron and proton densities have different profiles. As a result, the root-mean-square radius of the nucleus does not simply scale as $A^{1/3}$. Therefore, the scaling properties of such an ion-ion potential (and, consequently, of the implied fusion barrier parameters) should be different than in standard ion-ion potentials. Providing parametrizations within such a framework would be useful. However, such a task is outside the scope of the present work.

Summarizing, we presented phenomenological expressions suitable for the parametrization of fusion barrier radii and heights predicted by analytic nuclear potentials. Compared to commonly used formulas, they were found to reproduce theoretical barrier parameters with a higher accuracy. The proposed expressions make explicit reference to the entrance channel mass asymmetry and the neutron excess degree of freedom of the projectile and target nucleus. The deduced coefficients make possible the

assessment of the importance of the neutron excess degree of freedom implied by each potential.

References

1. *Proceedings of the Fourth International Conference on Radioactive Nuclear Beams, Omiya, Japan, 3-7 June, 1996*, edited by S. Kubono, T. Kobayashi, I. Tanihata, Nucl. Phys. A **616** (1997).
2. *Proceedings of the International Workshop on Fusion Dynamics at the Extremes, Dubna, Russia, 25-27 May, 2000*, edited by Y.T. Oganessian, V.I. Zagrebaev (World Scientific, 2001).
3. L.C. Vaz, J.M. Alexander, G.R. Satchler, Phys. Rep. **69**, 373 (1981).
4. D.G. Kovar, D.F. Geesaman, T.H. Braid, Y. Eisen, W. Henning, T.R. Ophel, M. Paul, K.E. Rehm, S.J. Sanders, P. Sperr, J.P. Schiffer, S.L. Tabor, S. Vigdor, B. Zeidman, F.W. Prosser jr., Phys. Rev. C **20**, 1305 (1979).
5. R.K. Puri, R.K. Gupta, Phys. Rev. C **45**, 1837 (1992).
6. R. Arora, R.K. Puri, R.K. Gupta, Eur. Phys. J. A **8**, 103 (2000).
7. P.R. Christensen, A. Winther, Phys. Lett. B **65**, 19 (1976).
8. R.K. Puri, M.K. Sharma, R.K. Gupta, Eur. Phys. J. A **3**, 277 (1998).
9. J.A. Christley, C.H. Dasso, S.M. Lenzi, M.A. Nagarajan, A. Vitturi, Nucl. Phys. A **587**, 390 (1995).
10. T.D. Thomas, Phys. Rev. **116**, 703 (1959).
11. R.A. Broglia, A. Winther, *Heavy Ion Reactions*, Vol. **1** (The Benjamin/Cummings Publishing Company, Inc., Reading, Massachusetts, 1981).
12. J. Blocki, J. Randrup, W.S. Swiatecki, C.F. Tsang, Ann. Phys. (N.Y.) **105**, 427 (1977).
13. J. Randrup, Nucl. Instrum. Methods **146**, 213 (1977).
14. H.J. Krappe, J.R. Nix, A.J. Sierk, Phys. Rev. Lett. **42**, 215 (1979).
15. H.J. Krappe, J.R. Nix, A.J. Sierk, Phys. Rev. C **20**, 992 (1979).
16. P. Möller, J.R. Nix, Nucl. Phys. A **361**, 117 (1981).
17. H. Ngô, Ch. Ngô, Nucl. Phys. A **348**, 140 (1980).